THE JOURNAL OF PHYSICAL CHEMISTRY Letters

pubs.acs.org/JPCL Letter

Ultrafast Spectroscopy of Lipid–Water Interfaces: Transmembrane Crowding Drives H-Bond Dynamics

Jennifer C. Flanagan, Alfredo E. Cardenas, and Carlos R. Baiz*

Cite This: J. Phys. Chem. Lett. 2020, 11, 4093–4098

Read Online

ACCESS | Metrics & More | Article Recommendations | Supporting Information

ABSTRACT: Biology takes place in crowded, heterogeneous environments, and it is therefore essential to account for crowding effects in our understanding of biophysical processes at the molecular level. Comparable to the cytosol, proteins occupy approximately 30% of the plasma membrane surface; thus, crowding should have an effect on the local structure and dynamics at the lipid–water interface. Using a combination of ultrafast two-dimensional infrared spectroscopy and molecular dynamics simulations, we quantify the effects of membrane peptide concentration on the picosecond interfacial H-bond dynamics. The measurements reveal a nonmonotonic dependence of water orientation and dynamics as a function of transmembrane peptide:lipid ratio. We observe three dynamical regimes: a "pure lipid-like" regime at low peptide concentrations, a bulk-like region at intermediate peptide concentrations where dynamics are faster by ∼20% compared to those of the pure lipid bilayer, and a crowded regime where high peptide concentrations slow dynamics by ∼50%.

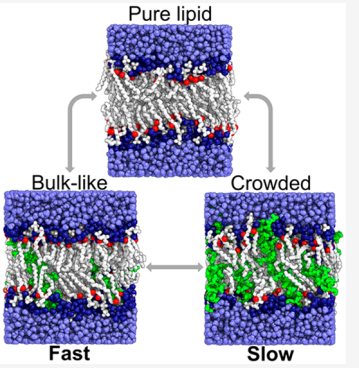

Biological processes such as protein folding, signaling, and diffusion take place in crowded heterogeneous environments. Much of the current focus of macromolecular crowding is oriented toward cytosolic crowding with a specific emphasis on its implications for folding stability and hydration of the protein environment in bulk aqueous environments.[1,2] Membrane models used in biophysical studies are often simplified, containing few lipid species and dilute concentrations of membrane proteins or peptides[3] such as the model shown in Figure 1A. In cells, plasma membranes are crowded and complex, containing high concentrations of transmembrane proteins such as ion channels and sensors.[4,5] Within this two-dimensional environment, the protein concentration is comparable to that of the cytosol, approximately 30% by area (compared to 30% by volume in the cytosol).[4−6] The average separation between membrane proteins can be as small as one or two lipid molecules.[5,6] Because cytosolic properties are significantly modulated by macromolecular crowding, membrane environments are also dictated by the structural and dynamical consequences of crowding.[3,7−9]

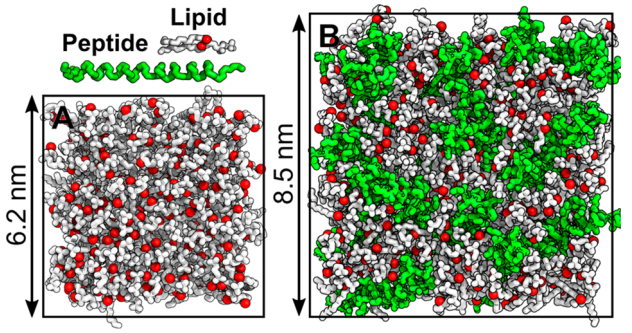

Figure 1. Representative model membranes used in MD simulations. (A) DMPC lipid bilayer without proteins. (B) Including transmembrane peptides in a 1:10 lipid:peptide ratio. Lipids are colored gray with the ester C═O oxygen atoms colored red. Peptide atoms are colored green.

Recent studies have explored this hypothesis, providing evidence of structural interruptions, domain formation, and diffusive motion as a consequence of membrane protein encounters approaching biological concentrations.[1,3,7,8,10,11] Key biological processes take place in interfacial environments, and thus, it is crucial to characterize the effect of crowding on the local environment at the interface between the hydrophobic and hydrophilic regions of the membrane from an atomistic perspective, including H-bond populations and dynamics.[12]

Two-dimensional infrared (2D IR) spectroscopy is an ideal tool for probing ultrafast dynamics at the lipid–water interface. The lipid ester C═O is precisely located at the ∼1 nm interface between hydrophobic and hydrophilic regions of the membrane, and their vibrational frequency is highly sensitive to its local electrostatic environment.[13−17] In short, 2D IR spectroscopy in the ester carbonyl region measures H-bond

Received: March 10, 2020
Accepted: May 3, 2020
Published: May 4, 2020

https://dx.doi.org/10.1021/acs.jpclett.0c00783
J. Phys. Chem. Lett. 2020, 11, 4093−4098

dynamics at the lipid−water interface on subpicosecond time scales.[8,18−23]

Where 2D IR offers direct dynamical information, computational tools, which map frequencies to atomic positions, provide a molecular interpretation of the underlying effects driving spectral dynamics. Expanding upon theoretical models developed over the past decade,[24−32] our group has recently developed a structure-based electrostatic map to accurately predict infrared spectra of ester C═O probes from classical molecular dynamics (MD) simulations.[14] Nearly quantitative agreement between time scales of computed and experimental frequency fluctuations shows that the simulations capture the essential interactions that lead to dynamics, and in these models, therefore the atomistic information contained in the simulation can be used to interpret experimental data.[33]

In this paper, we directly characterize the picosecond H-bond dynamics at the lipid−water interface in dimyristoyl-*sn*-glycero-3-phosphocholine (DMPC) bilayers using a range of concentrations of pH (low) insertion peptide (pHLIP), an amphiphilic helical transmembrane peptide that serves as a "crowder" in the membrane. Through the combined spectroscopic and computational approach, we characterize the water H-bond structure and dynamics at the lipid−water interface, providing an atomistic basis for understanding the specific effects of membrane crowding on interfacial processes in cells.

The pHLIP peptide is incorporated into ∼150 nm diameter DMPC lipid vesicles in solution. The peptide:lipid ratio is varied from pure DMPC to a 1:10 (crowded) ratio. The peptide is confirmed to remain in a helical conformation at different concentrations using circular dichroism (section S1). Control experiments indicate that the vesicles and the peptide structure are unperturbed with an increase in the pHLIP concentration in the membrane. The sample preparation and characterization protocols are provided in sections S1 and S2. The vesicles are prepared in a buffer at pH 8 and then spiked with a peptide solution, followed by a decrease in the pH. Because the insertion coordinate determines the final orientation, the helices are oriented in the same direction across the bilayer.[34] Considering that pHLIP contains a higher proportion of polar residues on the C-terminus, the dynamics of the two leaflets may be different. Experiments and simulations track the average dynamics over both leaflets.

We focus our analysis on the dynamics extracted from 2D IR experiments, which describe frequency correlations over vibrational time scales. We use molecular dynamics simulations to further interpret these dynamics from a structural perspective.

H-Bond Dynamics: 2D IR Spectroscopy. 2D IR spectra for DMPC, 1:50 lipid/peptide, and 1:10 lipid/peptide samples at selected waiting times are given in Figure 2. Each 2D IR spectrum consists of an excitation axis (horizontal) and a detection axis (vertical). Each peak appears as a positive/negative (red/blue) doublet where the positive peak on the diagonal originates from the ground state bleach and the negative, below-diagonal peak stems from excited state absorption. The ester C═O stretching mode is centered around 1730 cm^{-1} and is the focus of our analysis as this mode is sensitive to the interfacial H-bond dynamics.

Dynamics in 2D IR spectra are contained within the diagonal elongation of the ester peak. Diagonally elongated peaks are a result of a high degree of correlation between the excitation and detection frequencies. Over longer waiting

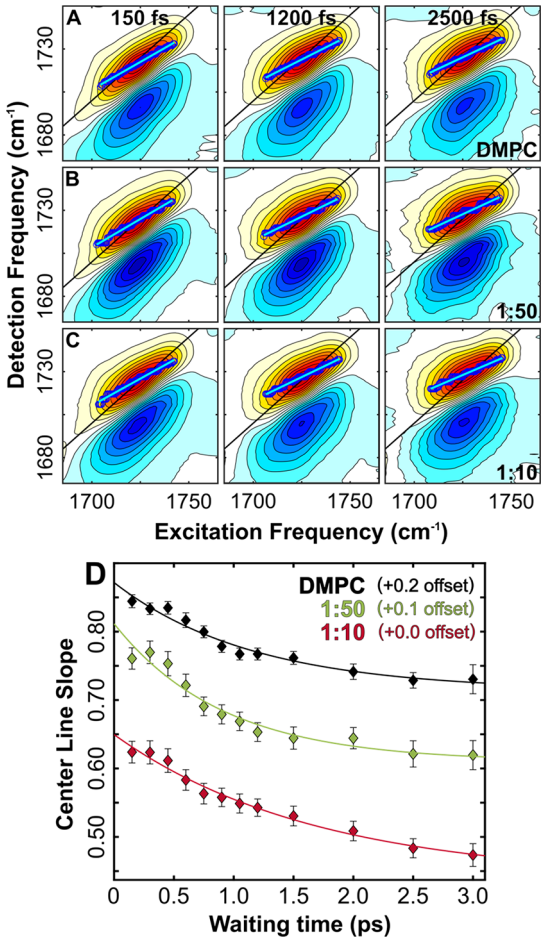

Figure 2. (A−C) Ester C═O 2D IR spectra of DMPC, 1:50 lipid/peptide, and 1:10 lipid/peptide samples, respectively, at waiting times of 150, 1200, and 2500 fs. Blue data points denote the maximum 2D IR intensities at each excitation frequency; light blue lines are the linear fits to these points from which the center-line slope is extracted. (D) CLS decays and exponential fits for the DMPC (black), 1:50 (green), and 1:10 (red) spectra. Decay *y*-axes are offset for the sake of clarity. Error bars represent the 95% confidence interval of the linear CLS fit. The center-line slope value is unitless.

times, oscillators sample a range of environments, leading to a rounder peak as the excitation-detection frequency correlation is lost; this is known as "spectral diffusion".[35] This loss of correlation can be quantified by a center-line slope (CLS) analysis, a widely used 2D IR analysis method that measures the diagonal elongation of the peak in each 2D IR spectrum.[36−38] Briefly, to compute the CLS, we identify the detection frequency at which the 2D IR intensity is maximized for each excitation frequency (blue points in Figure 2A−C). A linear fit to these points reveals the center-line slope (light blue lines, Figure 2A−C). Center-line slopes are plotted as a function of the excitation-detection delay and are fit to a monoexponential (Figure 2D and Figure S6). This CLS decay is exactly equivalent to measuring the ensemble-averaged frequency−frequency correlation function (FFCF) of the carbonyls. Faster relaxation rates are associated with more dynamic, bulk-like environments, whereas slower relaxation rates are consistent with more static environments.

The ∼1 ps decay captured by the CLS is commonly associated with H-bonding dynamics, which occur on this time scale.[39−41] These picosecond-scale dynamics account for

https://dx.doi.org/10.1021/acs.jpclett.0c00783
J. Phys. Chem. Lett. 2020, 11, 4093−4098

~20% of the overall spectral diffusion; also present are rapid, femtosecond-scale fluctuations, which cannot be captured by this experiment as they occur on time scales comparable to the laser pulse length (<100 fs), and long-time-scale (≳5 ps) fluctuations, which are represented by the constant offset in the CLS decay. The latter, known as static inhomogeneity,[42,43] is attributed to slow dynamics such as lateral diffusion, H-bond network reorganization, and transient peptide folding and insertion that occur over a wide range of time scales.[44,45] The remainder of this analysis focuses on the picosecond fluctuations, which reveal the H-bond dynamics. Full 2D IR data sets and associated CLS fits are given in the Supporting Information (section S2 and Figures S15−S22).

Figure 4A shows the CLS lifetimes for peptide:lipid ratios from 1:10 to pure lipid. Surprisingly, the relaxation rates do not exhibit a monotonic trend. The relaxation rate for the pure lipid bilayer is 1.19 ps, in agreement with previous measurements.[15] An increasing peptide concentration initially produces a slight slowing of dynamics, as observed in the 1:70 sample, although the relaxation rates are similar within experimental uncertainty. In the 1:50 peptide/lipid membrane, the dynamics are observed to be faster than in the pure lipid membrane. While changes between the low and intermediate regimes are small, the dynamics are different within the uncertainty of the 2D IR measurements. At peptide concentrations approaching highly crowded (near-biological) environments, dynamics are significantly slowed, with the 1:10 peptide/lipid mixture exhibiting a 1.75 ps relaxation rate, nearly 50% slower than the pure lipid membrane.

The "slow−fast−slow" dynamics observed with an increasing peptide concentration suggest the existence of three regimes: (1) a "pure lipid-like" regime at low peptide concentrations, (2) a "bulk-like" regime at intermediate concentrations, and (3) a "crowded" regime, where the high peptide concentration drives slow dynamics.[2] Next we evaluate these structural hypotheses through MD simulations.

H-Bond Dynamics: MD Simulations. Frequency−frequency correlation function (FFCF) decays of the lipid ester C═O probes are computed from MD simulations (Figure 3B) using a vibrational map that converts the electric field at each of the O−C═O atomic positions into a frequency shift.[14] MD snapshots stored every 20 fs are used to generate a frequency trajectory for each carbonyl, and each autocorrelation (Figure S9) is then fit to a triple-exponential function as described in Figure S3a. Three time scales are observed, a fast inertial decay of <0.1 ps, an ~1 ps decay, and a long ~8 ps decay. Our experiments are sensitive to only the ~1 ps relaxation time scales. Indeed, these picosecond decay constants can be directly compared to the experimental CLS time constants. Experiment and simulation are in nearly quantitative agreement (Figure 3). In the pure lipid membrane, the decay time is 0.97 ps compared to 1.19 ps for the 2D IR experiment. Similar to experiment, we observe nonmonotonic trends in relaxation rates. A low peptide concentration results in slowed dynamics compared to those of the pure lipid; intermediate concentrations result in fast, bulk-like dynamics compared to the pure lipid, and at high (1:10 peptide:lipid ratio) peptide concentrations, we observe dynamics approximately 30% slower than in the pure lipid membrane. Differences in dynamics at different concentrations are less pronounced in the MD, and the peptide:lipid ratio at which the fastest dynamics are observed is 1:70 in MD compared to 1:50 in experiment. Given that the MD simulations reproduce the experimental trend in C═O dynamics, we then use the MD trajectories to explore the contribution of different components to the C═O dynamics.

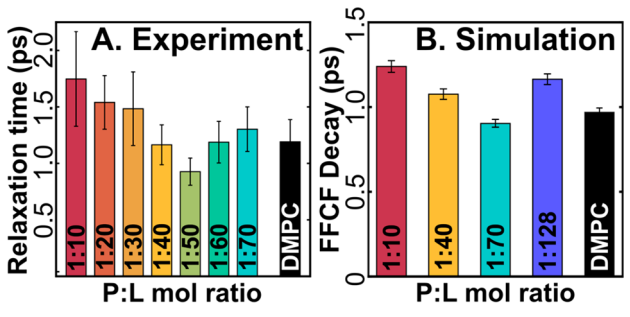

Figure 3. (A) Experimental decay constants of the frequency fluctuations extracted from a single-exponential fit of the center-line slope (CLS) for a range of lipid:peptide ratios (Figure S6). Error bars are generated by the bootstrap standard deviation with 1000 samples. (B) Frequency−frequency correlation function (FFCF) decay constants extracted by exponential fits of the FFCF from the MD simulations (Figure S9). Error bars represent the 95% confidence interval of the exponential fit.

Because frequency fluctuations result from the rapidly evolving electrostatic environment at the carbonyl positions, we can disentangle the origin of these fluctuations by computing the individual contributions to the frequency shifts separately. These include contributions from lipid, peptide, and water. This is accomplished by ignoring the contribution from the charges of individual components in the electrostatic computation prior to applying the frequency map. These analyses (Figure S8) indicate that the motions of the peptide molecules are not directly responsible for the observed frequency fluctuation trends, and the motions of the lipid molecules have only a minor effect. Rather, we determine the water component to be the origin of the frequency fluctuations given that the trend becomes inconsistent with experiment once the water charges are ignored. Thus, we focus our analysis on the water structure and dynamics at the membrane interface in relation to the bulk.

Considering that the interfacial dynamics at the C═O positions are primarily driven by H-bond dynamics, we computed the water−water solvent H-bond lifetimes. Geometric criteria, which are well established in the literature, are used to define H-bonds.[46,47] In brief, an H-bond is defined as an acceptor−donor pair within a 0.35 nm radius of one another, where the acceptor−donor−H angle is <30°. It is noteworthy that within this definition, H-bond populations are unchanged over the range of peptide concentrations (Figure S11). Water−water H-bond lifetimes are extracted from MD trajectories for interfacial and bulk water, defined as waters <1 and >1 nm from the nearest lipid C═O oxygen atom, respectively (Figure 4A). These cutoffs were selected as the peptide extends approximately 1 nm past the lipid carbonyls. Interfacial waters show overall longer lifetimes (>0.4 ps) compared to those of bulk waters (~0.3 ps), as expected, because the polarity of lipid headgroups orders the water molecules at the surface.[17,48] The interfacial H-bond lifetimes reproduce the "slow−fast−slow" trends derived from experiment (Figure 3A), wherein a low peptide:lipid ratio drives slowed dynamics, an intermediate peptide:lipid ratio results in rapid, near-bulk-like water dynamics, and the slowest water−water hydrogen bond lifetimes are found at high peptide

https://dx.doi.org/10.1021/acs.jpclett.0c00783
J. Phys. Chem. Lett. 2020, 11, 4093−4098

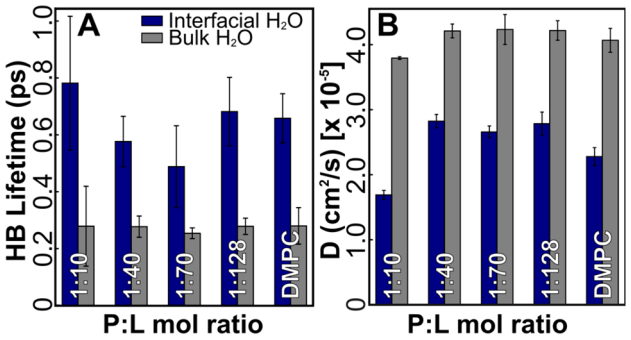

Figure 4. Water dynamics from simulation (gray, bulk water >1 nm from a lipid; blue, interfacial waters <1 nm from a lipid). (A) Water−water hydrogen bond lifetimes. (B) Self-diffusion coefficients.

concentrations. These results strongly indicate that the peptide therefore disrupts the H-bond networks at the interface, inducing faster, "bulk-like" dynamics at intermediate concentrations.

As further evidence, we computed the self-diffusion coefficients of interfacial and bulk water, shown Figure 4B, to describe the behavior of water in crowded environments. In this case, water diffusion expectedly follows the same trend as H-bond lifetimes: diffusion is faster in bulk water than at the interface, and interfacial water tracks the experimental trends in dynamics. Slowed water diffusion in crowded environments is a phenomenon that has been observed previously.[2] Feig et al. assigned the origin of this slow diffusion to a confined water environment compounded by interactions of water with multiple nearby proteins.[2] Furthermore, we can deduce that these altered water dynamics are projected onto the lipid−water interface and can be experimentally tractable by ultrafast spectroscopy.

To understand the structural origin of these trends, we next explore the H-bond geometries and orientations of interfacial waters.[17] Briefly, we select a subset of lipids with ester C═O oxygens within 1 nm of the nearest peptide C_α atom and analyze the water molecules within the 0.35 nm radius of the C═O oxygen atom, corresponding to the first solvation shell. Within this 0.35 nm radius, we compute the H−donor−acceptor (H−D−A) angle of the selected water molecules. H-Bond angle histograms in Figure 5 (normalized and offset for

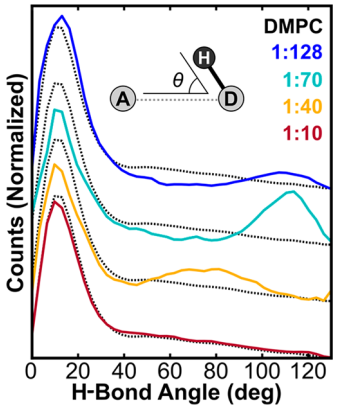

Figure 5. Histogram of A−D−H angles among lipid C═O and water molecules within an acceptor−donor radius of 0.35 nm. Dashed lines indicate the distribution for a pure lipid membrane; solid colored lines correspond to varied concentrations of the inserted peptide.

the sake of clarity) show a population between 0° and 30° that represents the water molecules forming hydrogen bonds to the lipids as both conditions of the H-bond definition are met. Beyond the 30° angle cutoff, these distributions deviate from the pure membrane system; upon introduction of the peptides, a second population emerges in a non-hydrogen bonding regime, suggesting the existence of water molecules that are present at the interface but unavailable for direct hydrogen bond interaction with the lipids.

The rapid water dynamics in the 1:70 peptide/lipid simulation system imply the existence of bulk-like water structure near the lipid−water interface, a phenomenon that has been reported previously.[12] These dynamics are corroborated by the distribution of water orientations given in Figure 5: unlike a pure lipid interface, where the water dipoles tend to be oriented antiparallel to the membrane normal,[17] which we will term "pure lipid-like" water, we observe a second discrete population of H−D−A angles within the C═O first solvation shell. In the 1:128 peptide/lipid membrane, we observe a smaller population with a similar 100−120° angle distribution. The bulk-like effect is diluted as the greater distance between peptides allows a larger fraction of the membrane surface to support pure lipid-like water. Reordering of the lipids as a consequence of peptide insertion is not captured by the water dynamics but likely drives the slowed dynamics of the FFCF decay observed in this regime.

On the contrary, C═O frequency fluctuations, water H-bond dynamics, and water diffusion rates are consistently slowed at crowded peptide concentrations (1:40 and 1:10 peptide:lipid regime). The high density of the transmembrane peptide interrupts H-bond networks, confining water to specific orientations. The 1:40 membrane shows an angle distribution distinct from the pure lipid-like and the bulk-like ensembles. In contrast, the 1:10 membrane has pure lipid-like water (Figure 5). Here, a greater fraction of the interfacial water is peptide-bound,[2] as we have previously demonstrated in this membrane peptide system.[49] Peptide-bound water exhibits slow dynamics compared to those of bulk water.[50] These two effects contribute to the slow FFCF decay we observe in 1:10 peptide/lipid samples. Interestingly, the 1:40 membrane water structure suggests a unique structural regime within this concentration range that cannot be described as a combination of the other two neighboring regimes. In conclusion, the combination of simulations and experiments suggests a strong link between water structure and lipid dynamics.

Our findings suggest three concurrent effects of an increased level of lipid membrane crowding by transmembrane peptides. (1) At low to intermediate peptide concentrations (up to 1:70 in simulation, up to 1:50 in experiment), interfacial water molecules adopt a bulk-like structure and rapid dynamics compared to those of a pure lipid system. (2) In a crowded, high-peptide concentration regime approaching biologically relevant transmembrane crowding, confined surface-like water leads to 30−50% slower dynamics at the interface. (3) A distinct set of water orientations exhibits moderately slowed dynamics in the intermediate regime approaching crowded lipid:peptide ratios, which cannot be described by the bulk-like or pure lipid-like water ensembles.

This study connects ultrafast dynamics to specific structural properties in the context of transmembrane crowding, providing a basis for perturbed lipid dynamics as a function of membrane peptide insertion. Our results indicate that there

https://dx.doi.org/10.1021/acs.jpclett.0c00783
J. Phys. Chem. Lett. 2020, 11, 4093−4098

is another level to understanding biomolecular crowding to fully comprehend the dense, complex domain that is the cellular environment. We have demonstrated that crowding affects membrane interfaces themselves and should be considered as part of a complete description of biomolecular environments in the cell.

MATERIALS AND METHODS

Below is a summary of the methods. Full descriptions can be found in the Supporting Information (section S1).

Sample Preparation. Unilamellar DMPC vesicles were prepared by reconstituting dried DMPC to 50 mM with 10 mM MOPS [3-(*N*-morpholino)propanesulfonic acid] buffer (pH 8.0) in D_2O and the appropriate volume of a pHLIP stock solution [5 mM in MOPS (pH 8.0)] to reach the desired DMPC:pHLIP mole ratio. After reconstitution, samples were sonicated at 30 °C for 15 min and then extruded with a 200 nm membrane to control the vesicle diameter. Each sample was adjusted to a final pH of 5.5 (uncorrected pH reading in D_2O).

2D IR Measurement. Two-dimensional IR spectra were recorded at 32 °C with a custom-built pulse-shaper-based spectrometer, which has been described in detail previously.[51] Spectra were recorded in the time domain at perpendicular polarization with varied population times (t_2) from 150 fs to 3 ps. Coherence times (t_1) were scanned up to 3 ps in 15 fs steps. Phase cycling was used to minimize contributions from scatter. Each 2D IR spectrum was averaged for 0.4 to 2.4 million laser shots depending on signal strength at the given t_2 value.

Molecular Dynamics. Classical MD simulations were run using GROMACS.[52] DMPC bilayers were prepared using the Membrane Builder[53,54] feature in CHARMM-GUI.[55,56] Fully protonated pHLIP helices were inserted evenly spaced into each bilayer to achieve the desired lipid:peptide ratio. Each model was equilibrated for 375 ps using the standard CHARMM-GUI protocol prior to production. Peptide-containing systems were run for 600−1400 ns, and the DMPC-only system was run for 200 ns, at 308.15 K in 2 fs steps. For spectral analysis, these trajectories were extending 1 ns saving coordinates every 20 fs. Electrostatic calculations were run using the final 300 ps of the simulation. Water MSD and A−D−H angles used the final 20 ps (1000 frames) after confirming convergence within this time frame. Water H-bond lifetime calculations used an average of six 20 ps (1000 frames) trajectories (see section S3).

ASSOCIATED CONTENT

Supporting Information

The Supporting Information is available free of charge at https://pubs.acs.org/doi/10.1021/acs.jpclett.0c00783.

Additional data, figures, and references (PDF)

AUTHOR INFORMATION

Corresponding Author

Carlos R. Baiz − *Department of Chemistry, The University of Texas at Austin, Austin, Texas 78712-1224, United States;* orcid.org/0000-0003-0699-8468; Email: cbaiz@cm.utexas.edu

Authors

Jennifer C. Flanagan − *Department of Chemistry, The University of Texas at Austin, Austin, Texas 78712-1224, United States*

Alfredo E. Cardenas − *Institute for Computational Engineering and Sciences, The University of Texas at Austin, Austin, Texas 78712-1224, United States*

Complete contact information is available at: https://pubs.acs.org/10.1021/acs.jpclett.0c00783

Notes

The authors declare no competing financial interest.

ACKNOWLEDGMENTS

This work has been supported by the Welch Foundation (F-1891) and the National Science Foundation (BIO-1815354). The authors acknowledge Professor Ron Elber (The University of Texas at Austin) for insightful discussions.

REFERENCES

(1) Zhou, H.-X.; Rivas, G.; Minton, A. P. Macromolecular Crowding and Confinement: Biochemical, Biophysical, and Potential Physiological Consequences. *Annu. Rev. Biophys.* **2008**, *37* (1), 375−397.

(2) Harada, R.; Sugita, Y.; Feig, M. Protein Crowding Affects Hydration Structure and Dynamics. *J. Am. Chem. Soc.* **2012**, *134* (10), 4842−4849.

(3) Guigas, G.; Weiss, M. Effects of Protein Crowding on Membrane Systems. *Biochim. Biophys. Acta, Biomembr.* **2016**, *1858* (10), 2441−2450.

(4) Engelman, D. M. Membranes Are More Mosaic than Fluid. *Nature* **2005**, *438* (7068), 578−580.

(5) Nicolson, G. L. The Fluid—Mosaic Model of Membrane Structure: Still Relevant to Understanding the Structure, Function and Dynamics of Biological Membranes after More than 40 Years. *Biochim. Biophys. Acta, Biomembr.* **2014**, *1838* (6), 1451−1466.

(6) Yeagle, P. L. Lipid Regulation of Cell Membrane Structure and Function. *FASEB J.* **1989**, *3* (7), 1833−1842.

(7) Sanderson, J. M. Resolving the Kinetics of Lipid, Protein and Peptide Diffusion in Membranes. *Mol. Membr. Biol.* **2012**, *29* (5), 118−143.

(8) Lee, E.; Kundu, A.; Jeon, J.; Cho, M. Water Hydrogen-Bonding Structure and Dynamics near Lipid Multibilayer Surface: Molecular Dynamics Simulation Study with Direct Experimental Comparison. *J. Chem. Phys.* **2019**, *151* (11), 114705.

(9) Dominguez, L.; Foster, L.; Straub, J. E.; Thirumalai, D. Impact of Membrane Lipid Composition on the Structure and Stability of the Transmembrane Domain of Amyloid Precursor Protein. *Proc. Natl. Acad. Sci. U. S. A.* **2016**, *113* (36), E5281−7.

(10) Verma, P. K.; Kundu, A.; Cho, M. How Molecular Crowding Differs from Macromolecular Crowding: A Femtosecond Mid-Infrared Pump−Probe Study. *J. Phys. Chem. Lett.* **2018**, *9* (22), 6584−6592.

(11) Ostrowska, N.; Feig, M.; Trylska, J. Modeling Crowded Environment in Molecular Simulations. *Front. Mol. Biosci.* **2019**, *6*, 86.

(12) Singh, P. C.; Inoue, K.; Nihonyanagi, S.; Yamaguchi, S.; Tahara, T. Femtosecond Hydrogen Bond Dynamics of Bulk-like and Bound Water at Positively and Negatively Charged Lipid Interfaces Revealed by 2D HD-VSFG Spectroscopy. *Angew. Chem., Int. Ed.* **2016**, *55* (36), 10621−10625.

(13) Stevenson, P.; Tokmakoff, A. Infrared Insights into the Effect of Cholesterol on Lipid Membranes. *Chem. Phys.* **2018**, *512*, 146−153.

(14) Edington, S. C.; Flanagan, J. C.; Baiz, C. R. An Empirical IR Frequency Map for Ester C = O Stretching Vibrations. *J. Phys. Chem. A* **2016**, *120* (22), 3888−3896.

(15) Valentine, M. L.; Cardenas, A. E.; Elber, R.; Baiz, C. R. Physiological Calcium Concentrations Slow Dynamics at the Lipid-Water Interface. *Biophys. J.* **2018**, *115* (8), 1541−1551.

(16) Seki, T.; Sun, S.; Zhong, K.; Yu, C.-C.; Machel, K.; Dreier, L. B.; Backus, E. H. G.; Bonn, M.; Nagata, Y. Unveiling Heterogeneity of Interfacial Water through the Water Bending Mode. *J. Phys. Chem. Lett.* **2019**, *10* (21), 6936−6941.
(17) Re, S.; Nishima, W.; Tahara, T.; Sugita, Y. Mosaic of Water Orientation Structures at a Neutral Zwitterionic Lipid/Water Interface Revealed by Molecular Dynamics Simulations. *J. Phys. Chem. Lett.* **2014**, *5* (24), 4343−4348.
(18) Kel, O.; Tamimi, A.; Thielges, M. C.; Fayer, M. D. Ultrafast Structural Dynamics Inside Planar Phospholipid Multibilayer Model Cell Membranes Measured with 2D IR Spectroscopy. *J. Am. Chem. Soc.* **2013**, *135* (30), 11063−11074.
(19) Park, S.; Kwak, K.; Fayer, M. D. Ultrafast 2D-IR Vibrational Echo Spectroscopy: A Probe of Molecular Dynamics. *Laser Phys. Lett.* **2007**, *4* (10), 704−718.
(20) Ghosh, A.; Ostrander, J. S.; Zanni, M. T. Watching Proteins Wiggle: Mapping Structures with Two-Dimensional Infrared Spectroscopy. *Chem. Rev.* **2017**, *117* (16), 10726−10759.
(21) Volkov, V. V.; Palmer, D. J.; Righini, R. Distinct Water Species Confined at the Interface of a Phospholipid Membrane. *Phys. Rev. Lett.* **2007**, *99* (7), 078302.
(22) Volkov, V. V.; Palmer, D. J.; Righini, R. Heterogeneity of Water at the Phospholipid Membrane Interface. *J. Phys. Chem. B* **2007**, *111*, 1377.
(23) Le Sueur, A. L.; Horness, R. E.; Thielges, M. C. Applications of Two-Dimensional Infrared Spectroscopy. *Analyst* **2015**, *140*, 4336.
(24) Reppert, M.; Tokmakoff, A. Computational Amide I 2D IR Spectroscopy as a Probe of Protein Structure and Dynamics. *Annu. Rev. Phys. Chem.* **2016**, *67* (1), 359−386.
(25) Jansen, T. la C.; Knoester, J. Nonadiabatic Effects in the Two-Dimensional Infrared Spectra of Peptides: Application to Alanine Dipeptide. *J. Phys. Chem. B* **2006**, *110*, 22910.
(26) Jansen, T.; Knoester, J. Waiting Time Dynamics in Two-Dimensional Infrared Spectroscopy. *Acc. Chem. Res.* **2009**, *42* (9), 1405−1411.
(27) Jansen, T.; Auer, B. M.; Yang, M.; Skinner, J. L. Two-Dimensional Infrared Spectroscopy and Ultrafast Anisotropy Decay of Water. *J. Chem. Phys.* **2010**, *132* (22), 224503.
(28) Liang, C.; Jansen, T. An Efficient N 3 -Scaling Propagation Scheme for Simulating Two-Dimensional Infrared and Visible Spectra. *J. Chem. Theory Comput.* **2012**, *8* (5), 1706−1713.
(29) Liang, C.; Louhivuori, M.; Marrink, S. J.; Jansen, T.; Knoester, J. Vibrational Spectra of a Mechanosensitive Channel. *J. Phys. Chem. Lett.* **2013**, *4* (3), 448−452.
(30) Reppert, M.; Tokmakoff, A. Electrostatic Frequency Shifts in Amide I Vibrational Spectra: Direct Parameterization against Experiment. *J. Chem. Phys.* **2013**, *138* (13), 134116.
(31) Reppert, M.; Roy, A. R.; Tokmakoff, A. Isotope-Enriched Protein Standards for Computational Amide I Spectroscopy. *J. Chem. Phys.* **2015**, *142* (12), 125104.
(32) Ghosh, A.; Ostrander, J. S.; Zanni, M. T. Watching Proteins Wiggle: Mapping Structures with Two-Dimensional Infrared Spectroscopy. *Chem. Rev.* **2017**, *117* (16), 10726−10759.
(33) Baryiames, C. P.; Teel, M.; Baiz, C. R. Interfacial H-Bond Dynamics in Reverse Micelles: The Role of Surfactant Heterogeneity. *Langmuir* **2019**, *35* (35), 11463−11470.
(34) Andreev, O. A.; Karabadzhak, A. G.; Weerakkody, D.; Andreev, G. O.; Engelman, D. M.; Reshetnyak, Y. K. PH (Low) Insertion Peptide (PHLIP) Inserts across a Lipid Bilayer as a Helix and Exits by a Different Path. *Proc. Natl. Acad. Sci. U. S. A.* **2010**, *107* (9), 4081−4086.
(35) Hamm, P.; Zanni, M. T. *Concepts and Methods of 2D Infrared Spectroscopy*; Cambridge University Press: Cambridge, U.K., 2011.
(36) Guo, Q.; Pagano, P.; Li, Y.-L.; Kohen, A.; Cheatum, C. M. Line Shape Analysis of Two-Dimensional Infrared Spectra. *J. Chem. Phys.* **2015**, *142* (21), 212427.
(37) Kwak, K.; Park, S.; Finkelstein, I. J.; Fayer, M. D. Frequency-Frequency Correlation Functions and Apodization in Two-Dimensional Infrared Vibrational Echo Spectroscopy: A New Approach. *J. Chem. Phys.* **2007**, *127* (12), 124503.
(38) Fenn, E. E.; Fayer, M. D. Extracting 2D IR Frequency-Frequency Correlation Functions from Two Component Systems. *J. Chem. Phys.* **2011**, *135* (7), 074502.
(39) Stevenson, P.; Tokmakoff, A. Ultrafast Fluctuations of High Amplitude Electric Fields in Lipid Membranes. *J. Am. Chem. Soc.* **2017**, *139* (13), 4743−4752.
(40) DeCamp, M. F.; DeFlores, L.; McCracken, J. M.; Tokmakoff, A.; Kwac, K.; Cho, M. Amide I Vibrational Dynamics of N-Methylacetamide in Polar Solvents: The Role of Electrostatic Interactions. *J. Phys. Chem. B* **2005**, *109*, 11016.
(41) Roberts, S. T.; Ramasesha, K.; Tokmakoff, A. Structural Rearrangements in Water Viewed Through Two-Dimensional Infrared Spectroscopy. *Acc. Chem. Res.* **2009**, *42* (9), 1239−1249.
(42) Tokmakoff, A. Two-Dimensional Line Shapes Derived from Coherent Third-Order Nonlinear Spectroscopy. *J. Phys. Chem. A* **2000**, *104*, 4247.
(43) Okumura, K.; Tokmakoff, A.; Tanimura, Y. Two-Dimensional Line-Shape Analysis of Photon-Echo Signal. *Chem. Phys. Lett.* **1999**, *314*, 488−495.
(44) Mouritsen, O. G.; Bagatolli, L. A. *Lipids in Bilayers—A Stress-Full and Busy Life*; Springer: Cham, Switzerland, 2016; pp 85−93.
(45) Elson, E. L.; Fried, E.; Dolbow, J. E.; Genin, G. M. Phase Separation in Biological Membranes: Integration of Theory and Experiment. *Annu. Rev. Biophys.* **2010**, *39*, 207−226.
(46) Baiz, C. R.; Tokmakoff, A. Structural Disorder of Folded Proteins: Isotope-Edited 2D IR Spectroscopy and Markov State Modeling. *Biophys. J.* **2015**, *108* (7), 1747−1757.
(47) Kim, Y. S.; Hochstrasser, R. M. Applications of 2D IR Spectroscopy to Peptides, Proteins, and Hydrogen-Bond Dynamics. *J. Phys. Chem. B* **2009**, *113*, 8231−8251.
(48) Mondal, J. A.; Nihonyanagi, S.; Yamaguchi, S.; Tahara, T. Three Distinct Water Structures at a Zwitterionic Lipid/Water Interface Revealed by Heterodyne-Detected Vibrational Sum Frequency Generation. *J. Am. Chem. Soc.* **2012**, *134* (18), 7842−7850.
(49) Flanagan, J. C.; Baiz, C. R. Site-Specific Peptide Probes Detect Buried Water in a Lipid Membrane. *Biophys. J.* **2019**, *116* (9), 1692−1700.
(50) Bellissent-Funel, M.-C.; Hassanali, A.; Havenith, M.; Henchman, R.; Pohl, P.; Sterpone, F.; van der Spoel, D.; Xu, Y.; Garcia, A. E. Water Determines the Structure and Dynamics of Proteins. *Chem. Rev.* **2016**, *116* (13), 7673−7697.
(51) Edington, S. C.; Gonzalez, A.; Middendorf, T. R.; Halling, D. B.; Aldrich, R. W.; Baiz, C. R. Coordination to Lanthanide Ions Distorts Binding Site Conformation in Calmodulin. *Proc. Natl. Acad. Sci. U. S. A.* **2018**, *115* (14), E3126−E3134.
(52) Abraham, M. J.; Murtola, T.; Schulz, R.; Páll, S.; Smith, J. C.; Hess, B.; Lindahl, E. GROMACS: High Performance Molecular Simulations through Multi-Level Parallelism from Laptops to Supercomputers. *SoftwareX* **2015**, *1−2*, 19−25.
(53) Jo, S.; Lim, J. B.; Klauda, J. B.; Im, W. CHARMM-GUI Membrane Builder for Mixed Bilayers and Its Application to Yeast Membranes. *Biophys. J.* **2009**, *97* (1), 50−58.
(54) Wu, E. L.; Cheng, X.; Jo, S.; Rui, H.; Song, K. C.; Dávila-Contreras, E. M.; Qi, Y.; Lee, J.; Monje-Galvan, V.; Venable, R. M.; et al. CHARMM-GUI *Membrane Builder* toward Realistic Biological Membrane Simulations. *J. Comput. Chem.* **2014**, *35* (27), 1997−2004.
(55) Jo, S.; Kim, T.; Iyer, V. G.; Im, W. CHARMM-GUI: A Web-Based Graphical User Interface for CHARMM. *J. Comput. Chem.* **2008**, *29* (11), 1859−1865.
(56) Lee, J.; Cheng, X.; Swails, J. M.; Yeom, M. S.; Eastman, P. K.; Lemkul, J. A.; Wei, S.; Buckner, J.; Jeong, J. C.; Qi, Y.; et al. CHARMM-GUI Input Generator for NAMD, GROMACS, AMBER, OpenMM, and CHARMM/OpenMM Simulations Using the CHARMM36 Additive Force Field. *J. Chem. Theory Comput.* **2016**, *12* (1), 405−413.

https://dx.doi.org/10.1021/acs.jpclett.0c00783
J. Phys. Chem. Lett. 2020, 11, 4093−4098